J Supercond Nov Magn (2012) 25:525–531
DOI 10.1007/s10948-011-1323-1

ORIGINAL PAPER

Structural, Magnetic and Microwave Properties of Eu-doped Barium Hexaferrite Powders

F. Khademi · A. Poorbafrani · P. Kameli · H. Salamati

Received: 21 August 2011 / Accepted: 22 September 2011 / Published online: 18 October 2011

Abstract Eu-doped M-type barium ferrite powders ($Ba_{1-x}Eu_xFe_{12}O_{19}$) with $x = 0.0$, 0.1, 0.2 and 0.25 were prepared by sol-gel method. The synthesized samples are characterized by thermo gravimetric analysis (TG-DTA), X-ray diffraction (XRD), Fourier transform infrared (FTIR) spectroscopy, scanning electron microscopy (SEM), vibrating sample magnetometer (VSM) and vector network analyzer. All the synthesized samples have the nearly single-magnetoplumbite phase. The results show that the crystallite size of doped samples is smaller than pure one. The saturation magnetization of doped ferrites decreases by the increase in Eu doping, while the coercivity increases. Maximum coercivity achieved in this study is 6.12 KOe for $x = 0.25$ sample. The enhancement of coercivity by Eu doping is mainly due to the higher magnetocrystalline anisotropy, which is attributed to the partial change of Fe^{+3} ion to Fe^{+2} ion. The maximum reflection loss (RL) of −43 dB at frequency range of 12–18 GHz for the $x = 0.1$ sample was obtained. The increase in reflection loss at higher frequency suggests that the Eu-doped sample can be used for the application in microwave devices.

Keywords Barium ferrite · Europium substitution · Magnetic properties · Microwave absorption

1 Introduction

Recently M-type hexagonal ferrites have attracted a lot of attention because of their magnetic properties such as a large magnetocrystalline anisotropy, high coercivity, great permeability and high magnetic resonance frequency. Due to the above mentioned properties, they have used extensively in chip inductor, high frequency devices, microwave absorber in GHz range, wireless communication tools and local area networks [1–6]. With the advancement of GHz electronic systems and telecommunications, the problem of the electromagnetic interface (EMI) has become a matter of serious concern and so much attention has been paid to find materials with suitable absorption property. For the purpose of preparing absorbing material, two fundamental conditions must be satisfied. The first is the matched characteristics impedance, in which intrinsic impedance of the material must be equal to the intrinsic impedance of free space. Second, the incident electromagnetic wave must enter and be attenuated entirely through the material [4, 7].

In order to improve the magnetic properties of M-type hexaferrites, there are several substituting Fe^{+3} and Sr^{+2}/Ba^{+2} with some cations such as La^{+3} [8], Pr^{+3} [9], Nd^{+3} [10], Sm^{+3} [11] and Dy^{+3} [12]. To vary the magnetic properties of M-type hexaferrites, rare earth elements are very unique because of their characteristic structure of electronic shells. The Lanthanides also improve the mechanical properties and hard magnetic properties of hexagonal ferrites [13, 14].

In this paper we studied the Eu substituted $BaFe_{12}O_{19}$ (BaM) ferrites prepared by sol-gel method. The aim of this work was to study their structural and magnetic properties, especially electromagnetic wave absorption behavior in GHz frequency range.

2 Experimental

The starting materials were barium nitrate ($Ba(NO_3)_2$), iron nitrate ($Fe(NO_3)_3{\cdot}9H_2O$), Europium oxide (Eu_2O_3), cit-

F. Khademi · A. Poorbafrani · P. Kameli (✉) · H. Salamati
Department of Physics, Isfahan University of Technology, Isfahan 84156-83111, Iran
e-mail: kameli@cc.iut.ac.ir

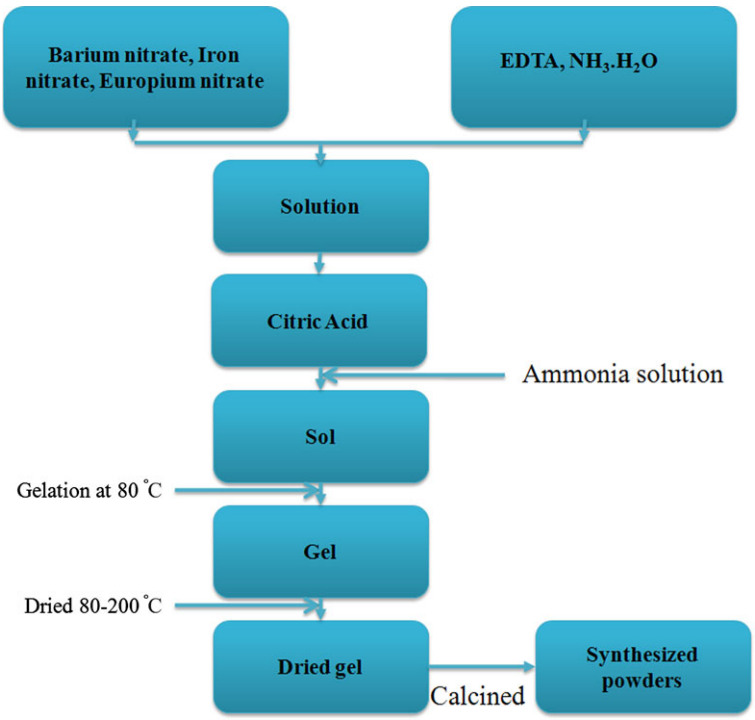

Fig. 1 The flow chart of synthesizing barium hexaferrite via sol-gel method

ric acid ($C_6H_8O_7{\cdot}H_2O$), ethylenediaminetetraacetic acid (EDTA) ($C_{10}H_{16}N_2O_8$) and ammonia solution, with analytically pure grade. In this method, citrate used as primary coordinate agent and suitable amount of EDTA was used as secondary coordinate agent that has stronger complexing ability. The cooperation of EDTA and citrate may result in more stable chelate complex [15]. In this report, the molar ratio of citric acid and EDTA: total metal cations were 1:1.

First, EDTA-$NH_3{\cdot}H_2O$ solution under stirring and heating was prepared. The required amounts of iron nitrate, barium nitrate and europium nitrate, which was prepared by the reaction between Eu_2O_3 and HNO_3, were dissolved in deionized water under stirring at 40 °C. After mixing dissolved citric acid into this solution, a homogeneous transparent aqueous solution was formed. Then aqueous NH_3 solution was added to the above solution to adjust pH value of the system around 7. The solutions were slowly evaporated at 80 °C until a highly viscose residue was formed. Increasing the temperature up to about 200 °C led to the obtained dried gel. Finally, the dried gel powders were calcinated in air at 1100 °C for 2 h with heating rate of 6 °C/min until 800 °C, and 3 °C/min from 800 °C to 1100 °C. The procedure is illustrated in Fig. 1.

The thermal decomposition behavior of sample was characterized by BAHR STA 503, TGA and DTA instruments, in air with the heating rate of 10 °C/min. The identification of the crystalline phase was carried out on Phillips XPERT X-ray Diffractometer using CuKα radiation. The FTIR spectra of the samples were done by Jasco 860 plus. XRF 2010 scanning electron microscope (SEM) was employed to get information about particle size and morphology. A vibrating sample magnetometer (Lakeshore 7400) used to determine magnetic behavior of samples at room temperature with an applied field of up to 20 kOe. The reflection loss of the samples was calculated using microwave network analyzer (ZVK).

3 Result and Discussion

3.1 Structural Properties

Figure 2 shows the TG-DTA plots, for the undoped sample. Dehydration, decomposition and sintering are common processes known to occur during heat treatment [16]. With the increase of temperature, there is no noticeable weightlessness in TG curve, and we have the exothermic peak at the temperature of higher than 850 °C in the DTA curve, indicating the formation of hexagonal phase. The weight loss below 500 °C and the endothermic peaks in the DTA curve are due to the loss of residual water in the gel and reaction of nitrates with citric acid. The main gaseous decomposition products are H_2O, CO, CO_2 and NO [17].

Thus, it is necessary to calcine the samples at temperatures higher than 850 °C. Therefore we calcined the samples at 1100 °C for 2 h. Figure 3 shows the XRD pattern of the samples. It can be seen that the samples are nearly single phase within the detection limit of the technique (JCPDS card no. 043-0002). The absence of other

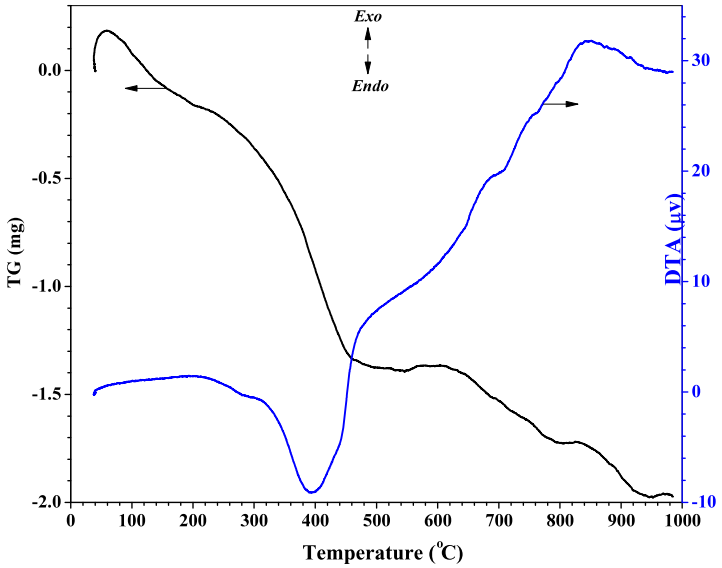

Fig. 2 TG-DTA curves of barium ferrite precursor

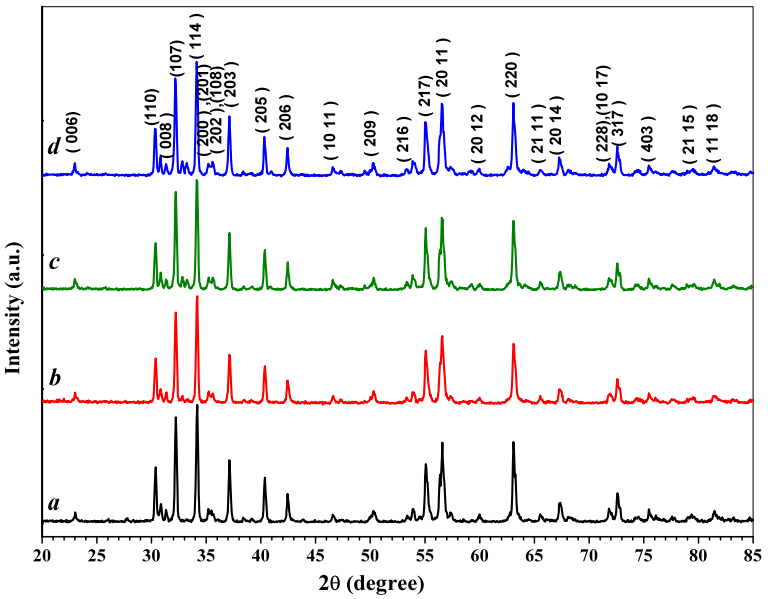

Fig. 3 XRD patterns of all Eu substituted ferrites sintered at 1100 °C, (**a**) $x = 0.0$, (**b**) $x = 0.1$, (**c**) $x = 0.2$ and (**d**) $x = 0.25$

phases in the doped ferrites suggests that Eu arranges in the hexagonal structure to fulfill the formation of single hexagonal phase. The peaks for doped Ba ferrites appear approximately at the same position as for the undoped ferrite.

The lattice constants, a and c are calculated according to the following equation [18]:

$$\frac{1}{d^2} = \frac{4}{3}\left(\frac{h^2 + hk + k^2}{a^2}\right) + \frac{l^2}{c^2}. \tag{1}$$

The lattice parameters of a (∼5.89 Å) and c (∼23.2 Å) remain almost constant without any particular trend of the variation.

The averages of crystallite size (D) of the samples were calculated from the main diffraction peaks using the Williamson–Hall formula [18]:

$$\beta \cos\theta = \frac{k\lambda}{D} + 2\varepsilon \sin\theta \tag{2}$$

where $\lambda = 1.54056$ Å is the X-ray wavelength, θ is the Bragg angle, β is the full width at half maximum of the main diffraction peaks which β and θ both expressed in radian and k is the constant equal to 0.9. The estimated D values are given in Table 1.

The results show that crystallite size of all doped barium ferrites is smaller than pure one. It is concluded that a rare

earth element, Eu, acts as a grain growth inhibitor, in agreement with other reports [19–21].

In Fig. 4 FTIR spectra indicate the absorption bands at 438, 553, 602 cm^{-1}, which is a characteristic bond of BaM, revealing the formation of BaM. The frequency band in the range 400–440 cm^{-1} and 580–610 cm^{-1} are due to the lattice vibrations of octahedral and tetrahedral metal ions, respectively [22]. The band at 1385 cm^{-1} is attributed to the characteristic band of NO_3^- and CO_2^- [23]. The samples show an absorption band centered at 3434 cm^{-1}, corresponding to hydrogen bonded O–H stretching. The absorption bond due to the bending mode of H_2O molecule around 1620 cm^{-1} is diagnostic of the presence of water of hydration [24]. There are no characteristic bonds of europium, as similar to XRD patterns. Band positions do not change significantly, because the change of Fe^{+3}–O^{2-} distances and lattice constant is not considerable by Eu doping.

Figure 5 shows SEM representative micrographs of the samples with $x = 0.0$ and 0.25. Particles with mean diameter

Table 1 Crystallite size, remanence, saturation magnetization and coercivity of $Ba_{1-x}Eu_xFe_{12}O_{19}$ samples with different values of substitution x

x	0.0	0.1	0.2	0.25
D (nm)	77	71	73	74
M_r (emu/gr)	35.66	37.26	35.29	34.52
M_s (emu/gr)	59.21	57.46	52.36	45.14
H_c (kOe)	1.92	2.44	4.81	6.12

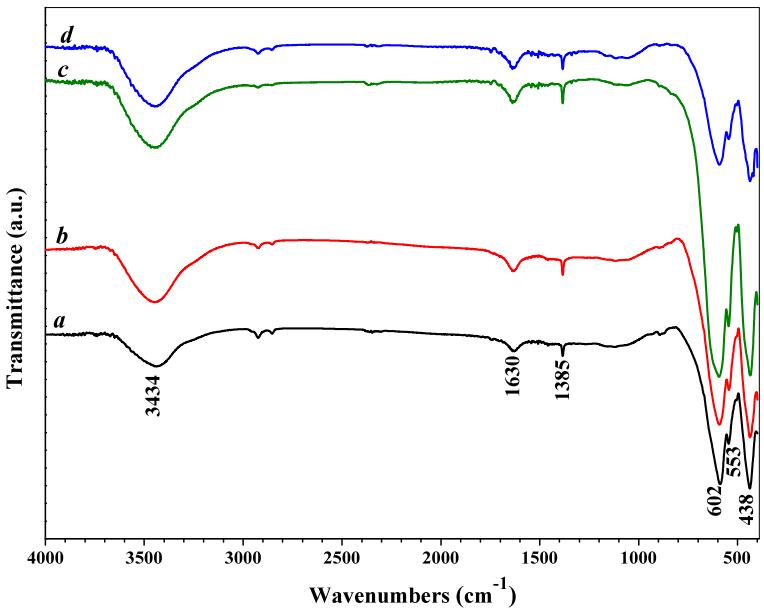

Fig. 4 FTIR spectra of Eu substituted ferrites, (**a**) $x = 0.0$, (**b**) $x = 0.1$, (**c**) $x = 0.2$ and (**d**) $x = 0.25$

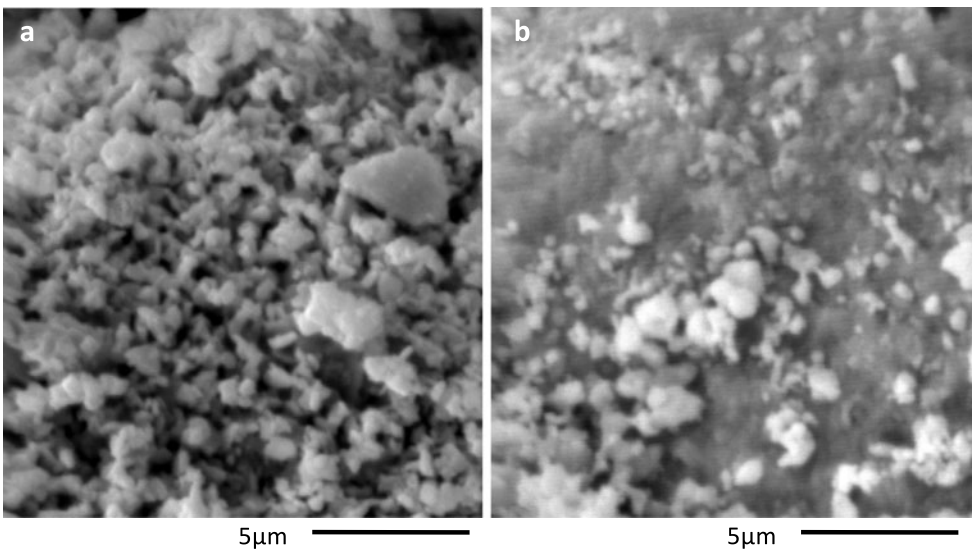

Fig. 5 SEM micrographs reveals morphology of (**a**) $x = 0.0$ and (**b**) $x = 0.25$ samples

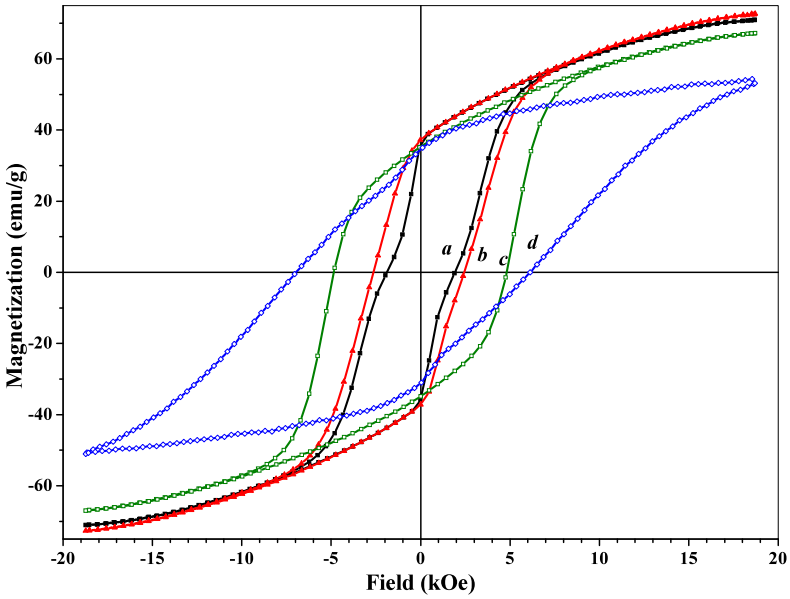

Fig. 6 Hysteresis loops of all Eu substituted samples, (**a**) $x = 0.0$, (**b**) $x = 0.1$, (**c**) $x = 0.2$ and (**d**) $x = 0.25$

of smaller than 1 μm along some particle agglomerations were observed in SEM images. The critical diameter of the barium ferrite with single magnetic domain is reported to be smaller than 1 μm [25]. So, the prepared ferrites are single domain. It seems that the small amount of Eu substitution will not affect the crystal structure and morphology of the samples significantly.

3.2 Magnetic Properties

The value of the coercive field and the saturation magnetization were measured at a maximum applied of 20 kOe at room temperature. Figure 6 indicates the M–H hysteresis loop of the samples. The value of saturation magnetization (M_s), remanence magnetization (M_r) and coercivity with Eu substitutions are summarized in Table 1. It can be seen that the M_s decreases by the increase of x. The minimum value of M_s, 45.14 emu/gr, obtained for $x = 0.25$. It is clear from a comparison of the values of H_c that the coercivity increases by the increase of Eu doping level. In order to explain the observed magnetic behaviors, we consider the BaM crystal structure. The BaM has hexagonal symmetry with space group $P6_3/mmc$ and 64 ions per cell located in 11 distinct basis sites. The Fe^{+3} ions are distributed on three octahedral sites (12k, $4f_2$ and 2a), one tetrahedral site ($4f_1$) and one trigonal bipyramidal site (2b). The spins in the 12k, 2a and 2b sites are parallel to each other, while the spins in the $4f_2$ and $4f_1$ sites are parallel to each other, point in the opposite direction with 12k, 2a and 2b sites. Accordingly, the net magnetic moment per formula can be expressed as [25]

$$m = 2a(\uparrow) + 2b(\uparrow) + 12k(\uparrow) + 4f_1(\downarrow) + 4f_2(\downarrow). \quad (3)$$

By substitution of the Ba^{+2} site with Eu^{+3} ions, some Fe^{+3} valence states change to Fe^{+2} states on 2a site. Since the magnetic moment of Fe^{+2} ions (4 μ_B) is less than Fe^{+3} ion (5 μ_B), magnetization of the samples decreases as Eu doping level increases. The enhancement of H_c is mainly due to the higher magnetocrystalline anisotropy, which is attributed to change of Fe^{+3} to Fe^{+2}. Also, the magnetic behavior of hexaferrite materials is governed by the strength of Fe^{+3}–Fe^{+3} exchange interactions [16]. The magnetic dilution and spin canting disrupt and weaken the Fe^{+3}–O–Fe^{+3} exchange interaction by Fe^{+2} ions and promote lower M_s.

We have measured the reflection loss of the samples in the X (8–12 GHz) and Ku (12–18 GHz) bands. According to transmittance line theory, the reflection loss of electromagnetic wave under normal incident wave in the case of a metal-back single layer is given by

$$RL\ (\mathrm{dB}) = 20\log\left|\frac{z_{in} - z_0}{z_{in} + z_0}\right|, \quad (4)$$

$$z_{in} = z_0\sqrt{\frac{\mu}{\varepsilon}}\tanh\left[j\frac{2\pi}{c}\sqrt{\mu\varepsilon}\,f\,d\right] \quad (5)$$

where z_0 is the characteristic impedance of free space, z_{in} is the input impedance of the metal backed microwave absorbing layer, $\mu = \mu' + j\mu''$ and $\varepsilon = \varepsilon' + j\varepsilon''$ are the complex permeability and permittivity of the composite medium, c is velocity of light in free space, f is the frequency and d is the thickness of the absorber. The impedance-matching condition is given by $z_{in} = z_0$ to represent perfect absorbing properties [26].

At high frequencies, ferromagnetic resonance caused to absorb microwave radiation. When the external microwave frequency is equal to or more than the frequency of ferromagnetic resonance, barium ferrite will absorb plenty of en-

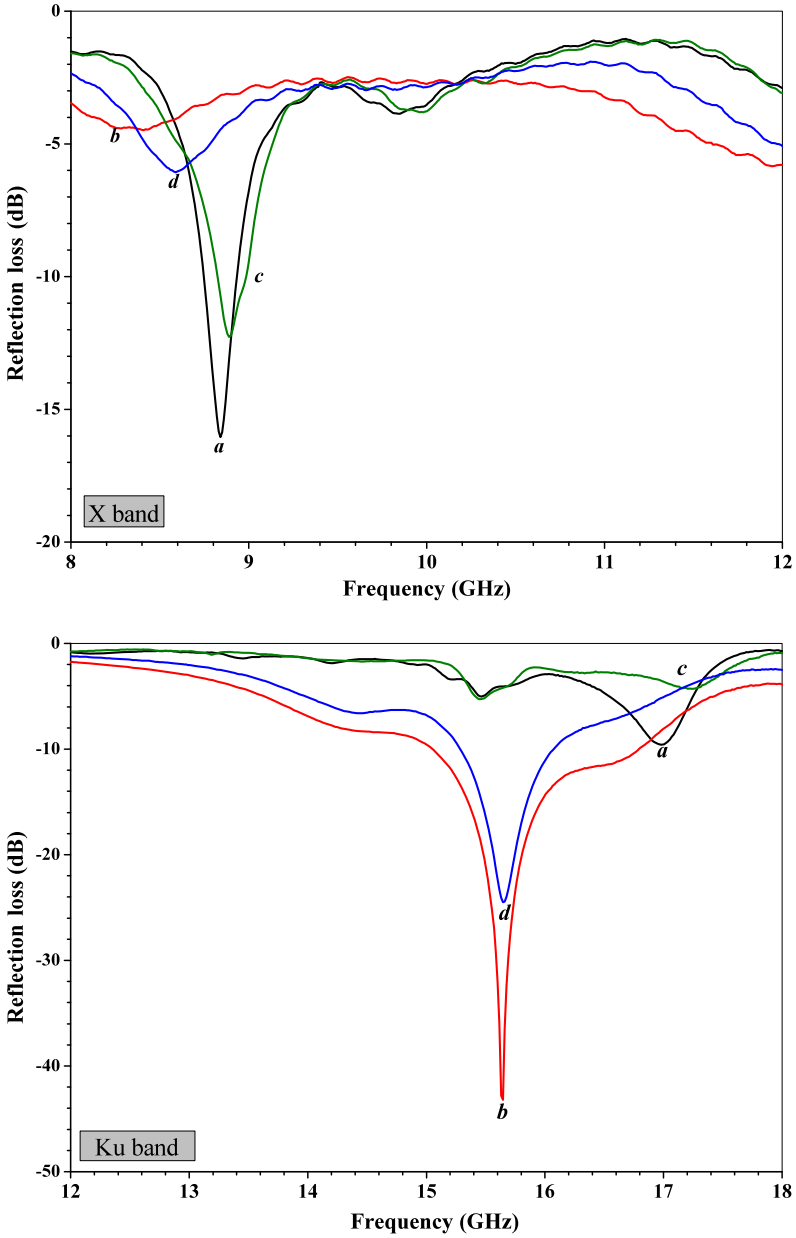

Fig. 7 Reflection loss vs. frequency for samples at X-band and Ku-band, (**a**) $x = 0.0$, (**b**) $x = 0.1$, (**c**) $x = 0.2$ and (**d**) $x = 0.25$

ergy. It is known that M-type hexagonal ferrite have a high resonance frequency that can be shifted to lower frequency by substituting [27].

Figure 7 represents the variation of reflection loss versus frequency with the thickness of 2 mm and 70% wt mass of composite ferrite with epoxy resin at X and Ku frequency bands, respectively. From the reflectivity curve at X band, it can be seen that undoped barium ferrite possesses better absorbing characteristics. The maximum reflection loss, −16 dB, can be achieved at 8.8 GHz. Also the resonance frequency shifted to lower frequency by the increase of Eu doping. As depicted in Fig. 7, in the Ku frequency band, the maximum reflection loss of −43 dB can be obtained by sample $x = 0.1$ at 15.6 GHz. It is well known that in case of single domain particles there is a reflection loss curve versus frequency due to the spin resonance [26]. As mentioned before, the samples prepared in this experiment are submicron sized and, consequently, are single magnetic domain. Therefore absorption takes place due to the magnetic spin resonance. Magnetic resonance arises as a result of the internal magnetic anisotropy field. Thus, the greatest microwave absorption for doped barium ferrite can be attributed to the interaction between magnetic ions and internal magnetic anisotropy field.

4 Conclusions

In summary, the Eu^{+3} doped barium hexaferrites have been prepared successfully by using the sol-gel method. X-ray

powder diffraction and FTIR spectra indicate a nearly single phased M-type structure for all samples. Pure and barium doped ferrites sintered at 1100 °C have particle size below 1 micrometer which demonstrate single domain structure. Substitution of Eu ions can be utilized for improvement of H_c, due to the enhancement of magnetocrystalline anisotropy. It was found that the M_r and M_s for all doped samples were lower than those of undoped samples. The magnetization behavior could be explained by considering the magnetic dilution and spin canting. The higher reflection loss for $x = 0.0$ sample in the X-band and for $x = 0.1$ sample in the Ku-band were obtained. Therefore, the ferrite with composition of $x = 0.1$ provides the best electromagnetic absorbing properties at Ku-band frequency and could be good candidate for practical applications at high frequency.

Acknowledgement The authors would like to thank Iran National Science Foundation (INSF) for supporting this project.

References

1. Iqbal, M.J., Ashiq, M.N., Hernandez-Gomez, P., Munoz Munoz, J.M., Cabrera, C.T.: J. Alloys Compd. **500**, 113 (2010)
2. Bsoul, I., Mahmood, S.H., Lehlooh, A.: J. Alloys Compd. **498**, 157 (2010)
3. Liu, Y., Drew, M., Liu, Y., Wang, J., Zhang, M.: J. Magn. Magn. Mater. **322**, 814 (2010)
4. Ghasemi, A., Saatchi, A., Salehi, M., Hossienpour, A., Morisako, A., Liu, X.: Phys. Status Solidi A **203**, 358 (2006)
5. Shahid, H., Nazar, A.S., Asghari, M., Abid, A., Muddasser, N., Waqar, A.A.: J. Supercond. Nov. Magn. **24**, 1245 (2011)
6. Geetanjali, Dube, C.L., Kashyap, S.C., Kotnala, R.K.: J. Supercond. Nov. Magn. **24**, 567 (2011)
7. Fannin, P.C., Marin, C.N., Malaescu, I., Stefu, N., Vlazan, P., Novaconi, S., Sfirloaga, P., Popescu, S., Couper, C.: Mater. Des. **32**, 1600 (2011)
8. Sozeri, H., Kucuk, I., Ozkan, H.: J. Supercond. Nov. Magn. **24**, 683 (2011)
9. Ounnunkad, S.: Solid State Commun. **138**, 472 (2006)
10. Sharma, P., Verma, A., Sidhu, R.K., Pandey, O.P.: J. Alloys Compd. **361**, 257 (2003)
11. Wang, J.F., Pontonb, C.B., Harris, I.R.: J. Magn. Magn. Mater. **234**, 233 (2001)
12. Litsardakis, G., Manolakis, I., Stergiou, A.C., Serletis, C., Efthimiadis, K.G.: IEEE Trans. Magn. **44**(11), 4222 (2008)
13. Rezlescu, N., Doroftei, C., Rezlescu, E., Popa, P.D.: J. Alloys Compd. **451**, 492 (2008)
14. Jalli, J., Hong, Y., Gee, S., Bae, S., Lee, J., Sur, J.C., Abo, G.S., Lyle, A., Lee, S., Lee, H., Mewes, T.: IEEE Trans. Magn. **44**(11), 2978 (2008)
15. Wang, L., Zhang, Q.: J. Alloys Compd. **469**, 251 (2009)
16. Iqbal, M.J., Farooq, S.: J. Alloys Compd. **505**, 560 (2010)
17. Mali, A., Ataie, A.: Ceram. Int. **30**, 1979 (2004)
18. Cullity, B.D.: Elements of X-ray Diffraction, 2nd edn. Addison-Wesly, Reading (1978)
19. Rai, G.M., Iqbal, M.A., Kubra, K.T.: J. Alloys Compd. **495**, 229 (2010)
20. Litsardakis, G., Manolakis, I., Serletis, C., Efthimiadis, K.G.: J. Magn. Magn. Mater. **310**, 884 (2007)
21. Lixi, W., Qiang, H., Lei, M., Qitu, Z.: J. Rare Earths **25**, 216 (2007)
22. Singhal, S., Namgyal, T., Singh, J., Chandra, K., Bansal, S.: Ceram. Int. **37**, 1833 (2011)
23. Koga, N., Tsutaoka, T.: J. Magn. Magn. Mater. **313**, 168 (2007)
24. Sudakar, C., Subbanna, G.N., Kutty, T.R.N.: J. Electroceram. **6**(2), 123 (2001)
25. Sozeri, H., Kucuk, I., Ozkan, H.: J. Magn. Magn. Mater. **323**, 1799 (2011)
26. Tabatabaie, F., Fathi, M.H., Saatchi, A., Ghasemi, A.: J. Alloys Compd. **474**, 206 (2009)
27. Ghasemi, A., Morisako, A.: J. Alloys Compd. **456**, 485 (2008)